

1 **MitoChime: A Machine-Learning Pipeline for**
2 **Detecting PCR-Induced Chimeras in**
3 **Mitochondrial Illumina Reads**

4 A Special Project Proposal
5 Presented to
6 the Faculty of the Division of Physical Sciences and Mathematics
7 College of Arts and Sciences
8 University of the Philippines Visayas
9 Miag-ao, Iloilo

10 In Partial Fulfillment
11 of the Requirements for the Degree of
12 Bachelor of Science in Computer Science

13 by

14 Duranne Duran
15 Yvonne Lin
16 Daniella Pailden

17 Adviser
18 Francis D. Dimzon, Ph.D.

19 December 5, 2025

Contents

21	1 Introduction	1
22	1.1 Overview	1
23	1.2 Problem Statement	3
24	1.3 Research Objectives	4
25	1.3.1 General Objective	4
26	1.3.2 Specific Objectives	4
27	1.4 Scope and Limitations of the Research	5
28	1.5 Significance of the Research	6
29	2 Review of Related Literature	7
30	2.1 The Mitochondrial Genome	7
31	2.1.1 Mitochondrial Genome Assembly	8

32	2.2 PCR Amplification and Chimera Formation	9
33	2.3 Existing Traditional Approaches for Chimera Detection	10
34	2.3.1 UCHIME	11
35	2.3.2 UCHIME2	12
36	2.3.3 CATch	13
37	2.3.4 ChimPipe	14
38	2.4 Machine Learning Approaches for Chimera and Sequence Quality	
39	Detection	15
40	2.4.1 Feature-Based Representations of Genomic Sequences . . .	16
41	2.5 Synthesis of Chimera Detection Approaches	17
42	3 Research Methodology	20
43	3.1 Research Activities	20
44	3.1.1 Data Collection	21
45	3.1.2 Feature Extraction Pipeline	25
46	3.1.3 Machine Learning Model Development	28
47	3.1.4 Model Benchmarking, Hyperparameter Optimization, and	
48	Evaluation	29
49	3.1.5 Feature Importance and Interpretation	31

50	3.1.6 Validation and Testing	32
51	3.1.7 Documentation	32
52	3.2 Calendar of Activities	33
53	4 Results and Discussion	34
54	4.1 Descriptive Analysis of Features	34
55	4.1.1 Univariate Distributions	35
56	4.2 Baseline Classification Performance	37
57	4.3 Effect of Hyperparameter Tuning	38
58	4.4 Detailed Evaluation of Representative Models	40
59	4.4.1 Confusion Matrices and Error Patterns	41
60	4.4.2 ROC and Precision–Recall Curves	42
61	4.5 Feature Importance and Biological Interpretation	44
62	4.5.1 Permutation Importance of Individual Features	44
63	4.5.2 Feature Family Importance	45
64	4.6 Summary of Findings	47

⁶⁵ List of Figures

⁶⁶	3.1 Process Diagram of Special Project	21
⁶⁷	4.1 Kernel density plots of six key features comparing clean and	
⁶⁸	chimeric reads.	36
⁶⁹	4.2 Test F1 of all baseline classifiers, showing that no single model	
⁷⁰	clearly dominates and several achieve comparable performance. . .	38
⁷¹	4.3 Comparison of test F1 (left) and ROC–AUC (right) for baseline and	
⁷²	tuned models. Hyperparameter tuning yields small but consistent	
⁷³	gains, particularly for tree-based ensembles.	40
⁷⁴	4.4 Confusion matrices for the four representative models on the held-	
⁷⁵	out test set. All models show more false negatives (chimeric reads	
⁷⁶	called clean) than false positives.	42
⁷⁷	4.5 ROC (left) and precision–recall (right) curves for the four represen-	
⁷⁸	tative models on the held-out test set. Tree-based ensembles cluster	
⁷⁹	closely, with logistic regression performing slightly but consistently	
⁸⁰	worse.	43

81	4.6 Permutation-based feature importance for four representative clas-	
82	sifiers. Clipping and k-mer composition features are generally the	
83	strongest predictors, whereas microhomology and other alignment	
84	metrics contribute minimally.	45
85	4.7 Aggregated feature family importance across four models. Clipping	
86	and k-mer compositional shifts are consistently the dominant con-	
87	tributors, while SA_structure, Micro_homology, and other features	
88	contribute minimally.	47

⁸⁹ List of Tables

⁹⁰	2.1 Comparison of Chimera Detection Methods	18
⁹¹	3.1 Timetable of Activities	33
⁹²	4.1 Performance of baseline classifiers on the held-out test set.	38
⁹³	4.2 Performance of tuned classifiers on the held-out test set.	39

⁹⁴ **Chapter 1**

⁹⁵ **Introduction**

⁹⁶ **1.1 Overview**

⁹⁷ The rapid advancement of next-generation sequencing (NGS) technologies has
⁹⁸ transformed genomic research by enabling high-throughput and cost-effective
⁹⁹ DNA analysis (Metzker, 2010). Among current platforms, Illumina sequencing
¹⁰⁰ remains the most widely adopted, capable of producing millions of short reads
¹⁰¹ that can be assembled into reference genomes or analyzed for genetic variation
¹⁰² (Bentley et al., 2008; Glenn, 2011). Despite its high base-calling accuracy,
¹⁰³ Illumina sequencing is prone to artifacts introduced during library preparation,
¹⁰⁴ particularly polymerase chain reaction (PCR)-induced chimeras, which are ar-
¹⁰⁵ tificial hybrid sequences that do not exist in the true genome (Judo, Wedel, &
¹⁰⁶ Wilson, 1998).

¹⁰⁷ PCR chimeras form when incomplete extension products from one template

anneal to an unrelated DNA fragment and are extended, creating recombinant reads (Qiu et al., 2001). In mitochondrial genome assembly, such artifacts are especially problematic because the mitochondrial genome is small, circular, and often repetitive (Boore, 1999; Cameron, 2014). Even a small number of chimeric or misjoined reads can reduce assembly contiguity and introduce false junctions during organelle genome reconstruction (Dierckxsens, Mardulyn, & Smits, 2017; Hahn, Bachmann, & Chevreux, 2013; Jin et al., 2020). Existing assembly tools such as GetOrganelle and MITObim assume that input reads are largely free of such artifacts (Hahn et al., 2013; Jin et al., 2020). Consequently, undetected chimeras may produce fragmented assemblies or misidentified organellar boundaries. To ensure accurate reconstruction of mitochondrial genomes, a reliable method for detecting and filtering PCR-induced chimeras before assembly is essential.

This study focuses on mitochondrial sequencing data from the genus *Sardinella*, a group of small pelagic fishes widely distributed in Philippine waters. Among them, *Sardinella lemuru* (Bali sardinella) is one of the country's most abundant and economically important species, providing protein and livelihood to coastal communities (Labrador, Agmata, Palermo, Ravago-Gotanco, & Pante, 2021; Willette, Bognot, Mutia, & Santos, 2011). Accurate mitochondrial assemblies are critical for understanding its population genetics, stock structure, and evolutionary history. However, assembly pipelines often encounter errors or fail to complete due to undetected chimeric reads. To address this gap, this research introduces MitoChime, a machine learning pipeline designed to detect and filter PCR-induced chimeric reads using both alignment-based and sequence-derived statistical features. The tool aims to provide bioinformatics laboratories, partic-

₁₃₃ ularly the Philippine Genome Center Visayas (PGC Visayas), with an efficient
₁₃₄ solution for improving mitochondrial genome reconstruction.

₁₃₅ 1.2 Problem Statement

₁₃₆ While NGS technologies have revolutionized genomic data acquisition, the ac-
₁₃₇ curacy of mitochondrial genome assembly remains limited by artifacts produced
₁₃₈ during PCR amplification. These chimeric reads can distort assembly graphs and
₁₃₉ cause misassemblies, with particularly severe effects in small, circular mitochon-
₁₄₀ drial genomes (Boore, 1999; Cameron, 2014). Existing assembly pipelines such
₁₄₁ as GetOrganelle, MITObim, and NOVOPlasty assume that sequencing reads are
₁₄₂ free of such artifacts (Dierckxsens et al., 2017; Hahn et al., 2013; Jin et al., 2020).
₁₄₃ At PGC Visayas, several mitochondrial assemblies have failed or yielded incom-
₁₄₄ plete contigs despite sufficient coverage, suggesting that undetected chimeric reads
₁₄₅ compromise assembly reliability. Meanwhile, existing chimera detection tools such
₁₄₆ as UCHIME and VSEARCH were developed primarily for amplicon-based com-
₁₄₇ munity analysis and rely heavily on reference or taxonomic comparisons (Edgar,
₁₄₈ Haas, Clemente, Quince, & Knight, 2011; Rognes, Flouri, Nichols, Quince, &
₁₄₉ Mahé, 2016). These approaches are unsuitable for single-species organellar data,
₁₅₀ where complete reference genomes are often unavailable. Therefore, there is a
₁₅₁ pressing need for a reference-independent, data-driven tool capable of detecting
₁₅₂ and filtering PCR-induced chimeras in mitochondrial sequencing datasets.

₁₅₃ **1.3 Research Objectives**

₁₅₄ **1.3.1 General Objective**

₁₅₅ This study aims to develop and evaluate a machine learning-based pipeline (Mi-
₁₅₆ toChime) that detects PCR-induced chimeric reads in *Sardinella lemuru* mito-
₁₅₇ chondrial sequencing data in order to improve the quality and reliability of down-
₁₅₈ stream mitochondrial genome assemblies.

₁₅₉ **1.3.2 Specific Objectives**

₁₆₀ Specifically, the study aims to:

- ₁₆₁ 1. construct simulated *Sardinella lemuru* Illumina paired-end datasets contain-
₁₆₂ ing both clean and PCR-induced chimeric reads,
- ₁₆₃ 2. extract alignment-based and sequence-based features such as k-mer compo-
₁₆₄ sition, junction complexity, and split-alignment counts from both clean and
₁₆₅ chimeric reads,
- ₁₆₆ 3. train, validate, and compare supervised machine-learning models for classi-
₁₆₇ fying reads as clean or chimeric,
- ₁₆₈ 4. determine feature importance and identify indicators of PCR-induced
₁₆₉ chimerism,
- ₁₇₀ 5. integrate the optimized classifier into a modular and interpretable pipeline
₁₇₁ deployable on standard computing environments at PGC Visayas.

172 1.4 Scope and Limitations of the Research

173 This study focuses on detecting PCR-induced chimeric reads in Illumina paired-
174 end mitochondrial sequencing data from *Sardinella lemuru*. The decision to re-
175 strict the taxonomic scope to a single species is based on four considerations:
176 (1) to limit interspecific variation in mitochondrial genome size, GC content, and
177 repetitive regions so that differences in read patterns can be attributed more di-
178 rectly to PCR-induced chimerism; (2) to align the analysis with relevant *S. lemuru*
179 sequencing projects at PGC Visayas; (3) to take advantage of the availability of *S.*
180 *lemuru* mitochondrial assemblies and raw datasets in public repositories such as
181 the National Center for Biotechnology Information (NCBI), which facilitates refer-
182 ence selection and benchmarking; and (4) to develop a tool that directly supports
183 local studies on *S. lemuru* population structure and fisheries management.

184 The study emphasizes `wgsim`-based simulations and selected empirical mito-
185 chondrial datasets from *S. lemuru*. It excludes naturally occurring chimeras, nu-
186 clear mitochondrial pseudogenes (NUMTs), and large-scale assembly rearrange-
187 ments in nuclear genomes. Feature extraction is restricted to low-dimensional
188 alignment and sequence statistics, such as k-mer frequency profiles, GC content,
189 read length, soft and hard clipping metrics, split-alignment counts, and map-
190 ping quality, rather than high-dimensional deep learning embeddings. This de-
191 sign keeps model behaviour interpretable and ensures that the pipeline can be
192 run on standard workstations at PGC Visayas. Testing on long-read platforms
193 (e.g., Nanopore, PacBio) and other taxa is outside the scope of this project; the
194 implemented pipeline is evaluated only on short-read *S. lemuru* datasets.

¹⁹⁵ **1.5 Significance of the Research**

¹⁹⁶ This research provides both methodological and practical contributions to mito-
¹⁹⁷ chondrial genomics and bioinformatics. First, MitoChime detects PCR-induced
¹⁹⁸ chimeric reads prior to genome assembly, with the goal of improving the con-
¹⁹⁹ tiguity and correctness of *Sardinella lemuru* mitochondrial assemblies. Second,
²⁰⁰ it replaces informal manual curation with a documented workflow, improving au-
²⁰¹ tomation and reproducibility. Third, the pipeline is designed to run on computing
²⁰² infrastructures commonly available in regional laboratories, enabling routine use
²⁰³ at facilities such as PGC Visayas. Finally, more reliable mitochondrial assemblies
²⁰⁴ for *S. lemuru* provide a stronger basis for downstream applications in the field of
²⁰⁵ fisheries and genomics.

²⁰⁶ **Chapter 2**

²⁰⁷ **Review of Related Literature**

²⁰⁸ This chapter presents an overview of the literature relevant to the study. It
²⁰⁹ discusses the biological and computational foundations underlying mitochondrial
²¹⁰ genome analysis and assembly, as well as existing tools, algorithms, and techniques
²¹¹ related to chimera detection and genome quality assessment. The chapter aims to
²¹² highlight the strengths, limitations, and research gaps in current approaches that
²¹³ motivate the development of the present study.

²¹⁴ **2.1 The Mitochondrial Genome**

²¹⁵ Mitochondrial genome (mtDNA) is a small, typically circular molecule found in
²¹⁶ most eukaryotes. It encodes essential genes involved in oxidative phosphorylation
²¹⁷ and energy metabolism. Because of its conserved structure, mtDNA has become
²¹⁸ a valuable genetic marker for studies in population genetics and phylogenetics
²¹⁹ (Anderson et al., 1981; Boore, 1999). In animal species, the mitochondrial genome

220 ranges from 15–20 kilobase and contains 13 protein-coding genes, 22 tRNAs, and
221 two rRNAs arranged compactly without introns (Gray, 2012). In comparison to
222 nuclear DNA, the ratio of the number of copies of mtDNA is higher and has
223 simple organization which make it particularly suitable for genome sequencing
224 and assembly studies (Dierckxsens et al., 2017).

225 **2.1.1 Mitochondrial Genome Assembly**

226 Mitochondrial genome assembly refers to the reconstruction of the complete mito-
227 chondrial DNA (mtDNA) sequence from raw or fragmented sequencing reads. It is
228 conducted to obtain high-quality, continuous representations of the mitochondrial
229 genome that can be used for a wide range of analyses, including species identi-
230 fication, phylogenetic reconstruction, evolutionary studies, and investigations of
231 mitochondrial diseases. Because mtDNA evolves rapidly, its assembled sequence
232 provides valuable insights into population structure, lineage divergence, and adap-
233 tive evolution across taxa (Boore, 1999). Compared to nuclear genome assembly,
234 assembling the mitochondrial genome is often considered more straightforward but
235 still encounters technical challenges such as the formation of chimeric reads. Com-
236 monly used tools for mitogenome assembly such as GetOrganelle and MITObim
237 operate under the assumption of organelle genome circularity, and are vulnerable
238 when chimeric reads disrupt this circular structure, resulting in assembly errors
239 (Hahn et al., 2013; Jin et al., 2020).

240 2.2 PCR Amplification and Chimera Formation

241 PCR plays an important role in NGS library preparation, as it amplifies target
242 DNA fragments for downstream analysis. However as previously mentioned, the
243 amplification process can also introduce chimeric reads which compromises the
244 quality of the input reads supplied to sequencing or assembly workflows. Chimeras
245 typically arise when incomplete extension occurs during a PCR cycle. This causes
246 the DNA polymerase to switch from one template to another and generate hy-
247 brid recombinant molecules (Judo et al., 1998). Artificial chimeras are produced
248 through such amplification errors, whereas biological chimeras occur naturally
249 through genomic rearrangements or transcriptional events.

250 In the context of amplicon-based sequencing, the presence of chimeras can in-
251 flate estimates of genetic or microbial diversity and may cause misassemblies dur-
252 ing genome reconstruction. Qin et al. (2023) has reported that chimeric sequences
253 may account for more than 10% of raw reads in amplicon datasets. This artifact
254 tends to be most prominent among rare operational taxonomic units (OTUs) or
255 singletons, which are sometimes misinterpreted as novel diversity, further caus-
256 ing the complication of microbial diversity analyses (Gonzalez, Zimmermann, &
257 Saiz-Jimenez, 2004). As such, determining and minimizing PCR-induced chimera
258 formation is vital for improving the quality of mitochondrial genome assemblies,
259 and ensuring the reliability of amplicon sequencing data.

260 2.3 Existing Traditional Approaches for Chimera

261 Detection

Several computational tools have been developed to identify chimeric sequences in NGS datasets. These tools generally fall into two categories: reference-based and de novo approaches. Reference-based chimera detection, also known as database-dependent detection, is one of the earliest and most widely used computational strategies for identifying chimeric sequences in amplicon-based community studies. These methods rely on the comparison of each query sequence against a curated, high-quality database of known, non-chimeric reference sequences (Edgar et al., 2011).

270 On the other hand, the de novo chimera detection, also referred to as reference-
271 free detection, represents an alternative computational paradigm that identifies
272 chimeric sequences without reliance on external reference databases. This method
273 infer chimeras based on internal relationships among the sequences present within
274 the dataset itself, making it particularly advantageous in studies of under explored
275 or taxonomically diverse communities where comprehensive reference databases
276 are unavailable or incomplete (Edgar, 2016; Edgar et al., 2011). The underlying
277 assumption on this method is that during PCR, true biological sequences are
278 generally more abundant as they are amplified early and dominate the read pool,
279 whereas chimeric sequences appear later and are generally less abundant. The
280 de novo approach leverage this abundance hierarchy, treating the most abundant
281 sequences as supposed parents and testing whether less abundant sequences can
282 be reconstructed as mosaics of these templates. Compositional and structural
283 similarity are also evaluated to check whether different regions of a candidate

284 sequence correspond to distinct high-abundance sequences.

285 In practice, many modern bioinformatics pipelines combine both paradigms
286 sequentially: an initial de novo step identifies dataset-specific chimeras, followed
287 by a reference-based pass that removes remaining artifacts relative to established
288 databases (Edgar, 2016). These two methods of detection form the foundation of
289 tools such as UCHIME and later UCHIME2.

290 2.3.1 UCHIME

291 UCHIME is one of the most widely used computational tools for detecting chimeric
292 sequences in amplicon sequencing data, as it serves as a critical quality control
293 step to prevent the misinterpretation of PCR artifacts as novel biological diversity.
294 The algorithm operates by searching for a model (M) where a query (Q) sequence
295 can be perfectly explained as a combination of two parent sequences, denoted as
296 A and B (Edgar et al., 2011).

297 In reference mode, UCHIME divides the query into four chunks and maps
298 them to a trusted chimeric-free database to identify candidate parents. It then
299 constructs a three-way alignment to calculate a score based on “votes.” A “Yes”
300 vote indicates the query aligns with parent A in one region and parent B in an-
301 other, while a “No” vote penalizes the score if the query diverges from the expected
302 chimeric model. In de novo mode, the algorithm operationalizes the abundance
303 skew principle described in Section 2.3. Instead of using an external database,
304 UCHIME dynamically treats the sample’s own high-abundance sequences as a
305 reference database, testing if lower-abundance sequences can be reconstructed as

306 mosaics of these internal ancestors (Edgar et al., 2011).

307 Despite its high sensitivity, UCHIME has inherent limitations rooted in
308 sequence divergence and database quality. The algorithm struggles to detect
309 chimeras formed from parents that are very closely related, specifically when the
310 sequence divergence between parents is less than roughly 0.8%, as the signal-to-
311 noise ratio becomes too low to distinguish a crossover event from sequencing error
312 (Edgar et al., 2011). Furthermore, in reference mode, the accuracy is strictly
313 bound by the completeness of the database; if true parents are absent, the tool
314 may fail to identify the chimera or produce false positives. Similarly, the de novo
315 mode relies on the assumption that parents are present and sufficiently more
316 abundant in the sample, which may not hold true in unevenly amplified samples
317 or complex communities.

318 2.3.2 UCHIME2

319 Building upon the original algorithm, UCHIME2 was developed to address the
320 nuances of high-resolution amplicon sequencing. A key contribution of the
321 UCHIME2 study was the critical re-evaluation of chimera detection benchmarks.
322 In the UCHIME2 paper (Edgar, 2016) and the UCHIME in practice website
323 (Edgar, n.d), the author has noted that the accuracy results reported in the
324 original UCHIME paper were “highly over-optimistic” because they relied on
325 unrealistic benchmark designs where parent sequences were assumed to be 100%
326 known and present. UCHIME2 introduced more rigorous testing (the CHSIMA
327 benchmark), revealing that “fake models,” where a valid biological sequence
328 perfectly mimics a chimera of two other valid sequences, are far more common

329 than previously assumed. This discovery suggests that error-free detection is
330 impossible in principle (Edgar, 2016). Another notable improvement is the in-
331 troduction of multiple application-specific modes that allow users to tailor the
332 algorithm’s performance to the characteristics of their datasets. The following
333 parameter presets: denoised, balanced, sensitive, specific, and high-confidence,
334 enable researchers to optimize the balance between sensitivity and specificity
335 according to the goals of their analysis.

336 However despite these advancements, the practical application of UCHIME2
337 requires caution. The author explicitly advises against using UCHIME2 as
338 a stand-alone tool in standard OTU clustering or denoising pipelines. Using
339 UCHIME2 as an independent filtering step in these workflows is discouraged, as
340 it often results in significantly higher error rates, increasing both false positives
341 (discarding valid sequences) and false negatives (retaining chimeras) (Edgar,
342 2016).

343 2.3.3 CATch

344 As previously mentioned, UCHIME (Edgar et al., 2011) relied on alignment-based
345 sequences in amplicon data. However, researchers soon observed that different al-
346 gorithms often produced inconsistent predictions. A sequence might be identified
347 as chimeric by one tool but classified as non-chimeric by another, resulting in
348 unreliable filtering outcomes across studies.

349 To address these inconsistencies, Mysara, Saeys, Leys, Raes, and Monsieurs
350 (2015) developed the Classifier for Amplicon Tool Chimeras (CATCh), which rep-

351 resents the first ensemble machine learning system designed for chimera detection
352 in 16S rRNA amplicon sequencing. Rather than depending on a single detec-
353 tion strategy, CATCh integrates the outputs of several established tools, includ-
354 ing UCHIME, ChimeraSlayer, DECIPHER, Pintail, and Perseus. The individual
355 scores and binary decisions generated by these tools are used as input features for
356 a supervised learning model. The algorithm employs a Support Vector Machine
357 (SVM) with a Pearson VII Universal Kernel (PUK) to determine optimal weight-
358 ings among the input features and to assign each sequence a probability of being
359 chimeric.

360 Benchmarking in both reference-based and de novo modes demonstrated signif-
361 icant performance improvements. CATCh achieved sensitivities of approximately
362 85 percent in reference-based mode and 92 percent in de novo mode, with corre-
363 sponding specificities of approximately 96 percent and 95 percent. These results
364 indicate that CATCh detected 7 to 12 percent more chimeras than any individual
365 algorithm while maintaining high precision.

366 2.3.4 ChimPipe

367 Among the available tools for chimera detection, ChimPipe is a pipeline developed
368 to identify chimeric sequences such as biological chimeras. It uses both discordant
369 paired-end reads and split-read alignments to improve the accuracy and sensitivity
370 of detecting biological chimeras (Rodriguez-Martin et al., 2017). By combining
371 these two sources of information, ChimPipe achieves better precision than meth-
372 ods that depend on a single type of indicator.

373 The pipeline works with many eukaryotic species that have available genome
374 and annotation data (Rodriguez-Martin et al., 2017). It can also predict multiple
375 isoforms for each gene pair and identify breakpoint coordinates that are useful
376 for reconstructing and verifying chimeric transcripts. Tests using both simulated
377 and real datasets have shown that ChimPipe maintains high accuracy and reliable
378 performance.

379 ChimPipe lets users adjust parameters to fit different sequencing protocols or
380 organism characteristics. Experimental results have confirmed that many chimeric
381 transcripts detected by the tool correspond to functional fusion proteins, demon-
382 strating its utility for understanding chimera biology and its potential applications
383 in disease research (Rodriguez-Martin et al., 2017).

384 **2.4 Machine Learning Approaches for Chimera 385 and Sequence Quality Detection**

386 Traditional chimera detection tools rely primarily on heuristic or alignment-based
387 rules. Recent advances in machine learning (ML) have demonstrated that models
388 trained on sequence-derived features can effectively capture compositional and
389 structural patterns in biological sequences. Although most existing ML systems
390 such as those used for antibiotic resistance prediction, taxonomic classification,
391 or viral identification are not specifically designed for chimera detection, they
392 highlight how data-driven models can outperform similarity-based heuristics by
393 learning intrinsic sequence signatures. In principle, ML frameworks can integrate
394 indicators such as k-mer frequencies, GC-content variation and split-alignment

395 metrics to identify subtle anomalies that may indicate a chimeric origin (Arango
396 et al., 2018; Liang, Bible, Liu, Zou, & Wei, 2020; Ren et al., 2020).

397 2.4.1 Feature-Based Representations of Genomic Sequences

398

399 Feature extraction converts DNA sequences into numerical representations suit-
400 able for machine-learning models. One approach is k-mer frequency analysis,
401 which counts short nucleotide sequences within a read (Vervier, Mahé, Tournoud,
402 Veyrieras, & Vert, 2015). High-frequency k-mers, including simple repeats such
403 as “AAAAAA,” can highlight repetitive or unusual regions that may occur near
404 chimeric junctions. Comparing k-mer patterns across adjacent parts of a read can
405 help identify such regions, while GC content provides an additional descriptor of
406 local sequence composition (Ren et al., 2020).

407 Alignment-derived features further inform junction detection. Long-read tools
408 such as Sniffles (Sedlazeck et al., 2018) use split alignments to locate breakpoints
409 across extended sequences, whereas short-read aligners like Minimap2 (Li, 2018)
410 report supplementary and secondary alignments that indicate local discontinu-
411 ities. Split alignments, where parts of a read map to different regions, can reveal
412 template-switching events. These features complement k-mer profiles and en-
413 hance detection of potentially chimeric reads, even in datasets with incomplete
414 references.

415 Microhomology, or short sequences shared between adjacent segments, is an-
416 other biologically meaningful feature. Its length, typically a few to tens of base

⁴¹⁷ pairs, has been linked to microhomology-mediated repair and template-switching
⁴¹⁸ mechanisms (Sfeir & Symington, 2015). In PCR-induced chimeras, short iden-
⁴¹⁹ tical sequences at junctions provide a clear signature of chimerism. Measuring
⁴²⁰ the longest exact overlap at each breakpoint complements k-mer and alignment
⁴²¹ features and helps identify reads that are potentially chimeric.

⁴²² 2.5 Synthesis of Chimera Detection Approaches

⁴²³ To provide an integrated overview of the literature discussed in this chapter, Ta-
⁴²⁴ ble 2.1 summarizes the major chimera detection studies, their methodological
⁴²⁵ approaches, and their known limitations.

Table 2.1: Comparison of Chimera Detection Methods

Methods	Approach	Limitations
Reference-based Chimera Detection	Compares query sequences against curated, non-chimeric reference databases; identifies mosaic sequences by evaluating similarity to known templates.	Depends heavily on completeness and quality of reference databases; often fails when novel taxa or missing parent sequences are present; reduced accuracy for low-divergence chimeras.
De novo Chimera Detection	Identifies chimeras using only internal dataset relationships; relies on abundance patterns and compositional similarity; reconstructs sequences as mosaics of high-abundance parents.	Assumes true sequences are more abundant—fails when amplification bias distorts abundance; struggles with evenly abundant parental sequences; can misclassify highly similar true variants.
UCHIME	Alignment-based chimera detection; segments query sequence, identifies parent candidates, performs 3-way alignment, and computes chimera scores; supports both reference-based and de novo modes.	Accuracy inflated in original benchmarks; suffers under incomplete databases; poor performance on low-divergence chimeras; sensitive to sequencing errors; misclassifies when parents are missing.
UCHIME2	Improved initial UCHIME benchmarking; offers multiple sensitivity/specificity modes; more robust with incomplete references; higher sensitivity.	Cannot achieve perfect accuracy due to “perfect fake models”; genuine variants may be indistinguishable from artificial recombinants; theoretical detection limit remains.
CATCh	First ML ensemble tool for 16S chimera detection; integrates outputs of UCHIME, ChimeraSlayer, DECI-PHER, Pintail, Perseus via SVM classifier; significantly improves sensitivity and specificity.	Depends on performance of underlying tools; ML model limited to features they output; ensemble can still misclassify in datasets with extreme novelty or low coverage.
ChimPipe	Pipeline for detecting fusion genes and transcript-derived chimeras in RNA-seq; uses discordant paired-end reads and split-alignments; predicts isoforms and breakpoint coordinates.	Designed for RNA-seq, not amplicons; needs high-quality genome and annotation; computationally heavier; limited to organisms with reference genomes.

426 Across existing studies, no single approach reliably detects all forms of chimeric
427 sequences, particularly those generated by PCR-induced template switching in
428 mitochondrial genomes. Reference-based tools perform poorly when parental se-
429 quences are absent; de novo methods rely strongly on abundance assumptions;
430 alignment-based systems show reduced sensitivity to low-divergence chimeras; and
431 ensemble methods inherit the limitations of their component algorithms. RNA-
432 seq-oriented pipelines likewise do not generalize well to organelle data. Although
433 machine learning approaches offer promising feature-based detection, they are
434 rarely applied to mitochondrial genomes and are not trained specifically on PCR-
435 induced organelle chimeras. These limitations indicate a clear research gap: the
436 need for a specialized, feature-driven classifier tailored to mitochondrial PCR-
437 induced chimeras that integrates k-mer composition, split-alignment signals, and
438 microhomology features to achieve more accurate detection than current heuristic
439 or alignment-based tools.

⁴⁴⁰ Chapter 3

⁴⁴¹ Research Methodology

⁴⁴² This chapter outlines the steps involved in completing the study, including data
⁴⁴³ gathering, generating simulated mitochondrial Illumina reads, preprocessing and
⁴⁴⁴ indexing the data, developing a feature extraction pipeline to extract key features,
⁴⁴⁵ applying machine learning algorithms for chimera detection, and validating and
⁴⁴⁶ comparing model performance.

⁴⁴⁷ 3.1 Research Activities

⁴⁴⁸ As illustrated in Figure 3.1, this study carried out a sequence of procedures to
⁴⁴⁹ detect PCR-induced chimeric reads in mitochondrial genomes. The process began
⁴⁵⁰ with collecting a mitochondrial reference sequence of *Sardinella lemuru* from the
⁴⁵¹ National Center for Biotechnology Information (NCBI) database, which was used
⁴⁵² as a reference for generating simulated clean and chimeric reads. These reads
⁴⁵³ were subsequently indexed and mapped. The resulting collections then passed

454 through a feature extraction pipeline that extracted k-mer profiles, supplementary
455 alignment (SA) features, and microhomology information to prepare the data for
456 model construction. The machine learning model was trained using the processed
457 input, and its precision and accuracy were assessed. It underwent tuning until it
458 reached the desired performance threshold, after which it proceeded to validation
459 and will undergo testing.

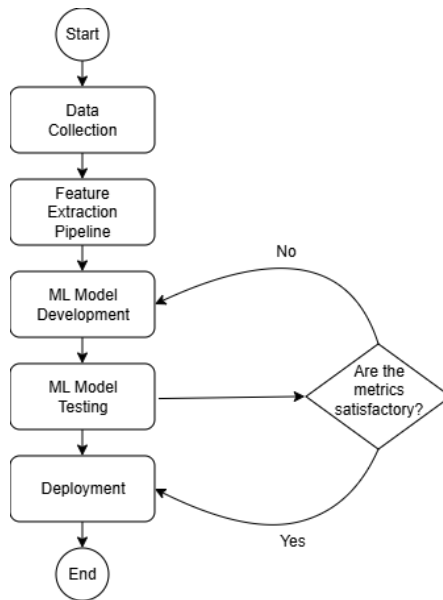


Figure 3.1: Process Diagram of Special Project

460 3.1.1 Data Collection

461 The mitochondrial genome reference sequence of *S. lemuru* was obtained from the
462 NCBI database (accession number NC_039553.1) in FASTA format. This sequence
463 served as the basis for generating simulated reads for model development.

464 This step was scheduled to begin in the first week of November 2025 and
465 expected to be completed by the end of that week, with a total duration of ap-

466 proximately one (1) week.

467 Data Preprocessing

468 To reduce manual repetition, all steps in the simulation and preprocessing pipeline
469 were executed using a custom script in Python (Version 3.11). The script runs
470 each stage, including read simulation, reference indexing, mapping, and alignment
471 processing, in a fixed sequence.

472 Sequencing data were simulated from the NCBI reference genome using `wgsim`
473 (Version 1.13). First, a total of 10,000 paired-end fragments were simulated,
474 producing 20,000 reads (10,000 forward and 10,000 reverse) from the the original
475 reference (`original_reference.fasta`) and and designated as clean reads using
476 the command:

```
477 wgsim -1 150 -2 150 -r 0 -R 0 -X 0 -e 0.001 -N 10000 \  
478     original_reference.fasta ref1.fastq ref2.fastq
```

479 The command parameters are as follows:

- 480 • `-1` and `-2`: read lengths of 150 base pairs for each paired-end read.
- 481 • `-r`, `-R`, `-X`: mutation rate, fraction of indels, and indel extension probability,
482 all set to a default value of 0.
- 483 • `-e`: base error rate, set to 0.001 to simulate realistic sequencing errors.
- 484 • `-N`: number of read pairs, set to 10,000.

485 Chimeric sequences were then generated from the same NCBI reference using a
486 separate Python script. Two non-adjacent segments were randomly selected such
487 that their midpoint distances fell within specified minimum and maximum thresh-
488 olds. The script attempts to retain microhomology, or short identical sequences
489 at segment junctions, to mimic PCR-induced template switching. The resulting
490 chimeras were written to `chimera_reference.fasta`, with headers recording seg-
491 ment positions and microhomology length. The `chimera_reference.fasta` was
492 processed with `wgsim` to simulate 10,000 paired-end fragments, generating 20,000
493 chimeric reads (10,000 forward reads in `chimeric1.fastq` and 10,000 reverse reads
494 in `chimeric2.fastq`) using the command format.

495 Next, a `minimap2` index of the reference genome was created using:

```
496 minimap2 -d ref.mmi original_reference.fasta
```

497 Minimap2 (Version 2.28) is a tool used to map reads to a reference genome.
498 The index `ref.mmi` of the original reference sequence is required by `minimap2` for
499 efficient read mapping. Mapping allows extraction of alignment features from each
500 read, which were used as input for the machine learning model. The simulated
501 clean and chimeric reads were then mapped to the reference index as follows:

```
502 minimap2 -ax sr -t 8 ref.mmi ref1.fastq ref2.fastq > clean.sam
```

```
503 minimap2 -ax sr -t 8 ref.mmi \  
504 chimeric1.fastq chimeric2.fastq > chimeric.sam
```

505 Here, `-ax sr` specifies short-read alignment mode, and `-t 8` uses 8 CPU

506 threads. The resulting clean and chimeric SAM files contain the alignment posi-
507 tions of each read relative to the original reference genome.

508 The SAM files were then converted to BAM format, sorted, and indexed using
509 `samtools` (Version 1.20):

```
510 samtools view -bS clean.sam -o clean.bam  
511 samtools view -bS chimeric.sam -o chimeric.bam  
512  
513 samtools sort clean.bam -o clean.sorted.bam  
514 samtools index clean.sorted.bam  
515  
516 samtools sort chimeric.bam -o chimeric.sorted.bam  
517 samtools index chimeric.sorted.bam
```

518 BAM files are the compressed binary version of SAM files, which enables faster
519 processing and reduced storage. Sorting arranges reads by genomic coordinates,
520 and indexing allows detection of SA as a feature for the machine learning model.

521 The total number of simulated reads was expected to be 40,000. The final col-
522 lection of reads contained 19,984 clean reads and 20,000 chimeric reads (39,984 en-
523 tries in total), providing a roughly balanced distribution between the two classes.
524 After alignment with `minimap2`, only 19,984 clean reads remained because un-
525 mapped reads were not included in the BAM file. Some sequences failed to align
526 due to the 5% error rate defined during `wgsim` simulation, which produced mis-
527 matches that caused certain reads to fall below the aligner's matching threshold.

528 This whole process is scheduled to start in the second week of November 2025

529 and is expected to be completed by the last week of November 2025, with a total
530 duration of approximately three (3) weeks.

531 **3.1.2 Feature Extraction Pipeline**

532 A feature extraction pipeline will be developed and implemented to extract the
533 necessary analytical features. This pipeline will function as a reproducible and
534 modular workflow that accepts FASTQ and BAM/SAM file inputs, processes them
535 using tools such as `samtools` and `jellyfish` (Version 2.3.1), and produces tabular
536 feature matrices (TSV) for downstream machine learning. To ensure correctness
537 and adherence to best practices, bioinformatics experts at the PGC Visayas will
538 be consulted to validate the pipeline design, feature extraction logic, and overall
539 data integrity. This stage of the study is scheduled to begin in the first week of
540 January 2026 and conclude by the last week of February 2026, with an estimated
541 total duration of approximately two (2) months.

542 The feature extraction pipeline focuses on three principal features from the
543 simulated and aligned sequencing data: (1) supplementary alignment flag (SA
544 count), (2) k-mer composition difference between read segments, and (3) micro-
545 homology length at potential junctions. Each of these features captures a distinct
546 biological or computational signature associated with PCR-induced chimeras.

547 **Supplementary Alignment Flag**

548 Supplementary alignment information will be assessed using the mapped and
549 sorted BAM files (`clean.sorted.bam` and `chimeric.sorted.bam`) generated

550 from the data preprocessing stage. Alignment summaries will be checked using
551 `samtools flagstat` to obtain preliminary quality-control statistics, including
552 counts of primary, secondary, and supplementary (SA) alignments.

553 Both BAM files will be converted to SAM format for detailed inspection of
554 reads in each file:

```
555 samtools view -h clean.sorted.bam -o clean.sorted.sam  
556 samtools view -h chimeric.sorted.bam -o chimeric.sorted.sam
```

557 The SAM output will be checked for reads containing the SA:Z flag, as it
558 denotes supplementary alignments. Reads exhibiting these or substantial soft-
559 clipped regions will be considered strong candidates for chimeric artifacts. A
560 custom Python script would be created to extract the alignment-derived features
561 and relevant metadata including mapping quality, SAM flag information, CIGAR-
562 based clipping, and alignment coordinates. These extracted attributes would then
563 be organized and compiled into a TSV (.tsv) file.

564 K-mer Composition Difference

565 Chimeric reads often comprise fragments from distinct genomic regions, resulting
566 in a compositional discontinuity between segments. Comparing k-mer frequency
567 profiles between the left and right halves of a read allows detection of such abrupt
568 compositional shifts, independent of alignment information. This will be obtained
569 using Jellyfish, a fast k-mer counting software. For each read, the sequence will
570 be divided into two segments, either at the midpoint or at empirically determined
571 breakpoints inferred from supplementary alignment data, to generate left and right

572 sequence segments. Jellyfish will then compute k-mer frequency profiles (with $k =$
573 5 or 6) for each segment. The resulting k-mer frequency vectors will be normalized
574 and compared using distance metrics such as cosine similarity or Jensen–Shannon
575 divergence to quantify compositional disparity between the two halves of the same
576 read. The resulting difference scores will be stored in a structured TSV file.

577 Microhomology

578 The microhomology length was computed as part of the feature extraction
579 pipeline. For each aligned read in the BAM files, the script first inferred a
580 breakpoint using the function `infer_breakpoint`, which represents a junction
581 between two segments. Breakpoints were determined primarily from soft-clipping
582 patterns, where part of a read does not align to the reference and may indicate
583 a junction. If no soft clips were present, SA tags were used to identify potential
584 alignment discontinuities.

585 Once a breakpoint was established, the script scanned a ± 40 base pair window
586 surrounding the breakpoint and used the function `longest_suffix_prefix_overlap`
587 to identify the longest exact suffix-prefix overlap between the left and right read
588 segments. This overlap, which represents consecutive bases shared at the junc-
589 tion, was recorded as the `microhomology_length` in the dataset. The 40-base
590 pair window was chosen to ensure that short shared sequences at or near the
591 breakpoint were captured, without including distant sequences that are unrelated.
592 Additionally, the GC content of the overlapping sequence was calculated using
593 the function `gc_content`, which counts guanine (G) and cytosine (C) bases within
594 the detected microhomology and divides by the total length, yielding a proportion

595 between 0 and 1, and was stored under the `microhomology_gc` attribute. Short
596 microhomologies, typically 3-20 base pairs in length, are recognized signatures of
597 PCR-induced template switching (Peccoud et al., 2018).

598 A k-mer length of 6 was used to capture patterns within the same 40-base pair
599 window surrounding each breakpoint. These profiles complement microhomology
600 measurements and help identify junctions that are potentially chimeric.

601 3.1.3 Machine Learning Model Development

602 After feature extraction, the per-read feature matrices for clean and chimeric
603 reads were merged into a single dataset. Each row corresponded to one paired-
604 end read, and columns encoded alignment-structure features (e.g., supplementary
605 alignment count and spacing between segments), CIGAR-derived soft-clipping
606 statistics (e.g., left and right soft-clipped length, total clipped bases), k-mer com-
607 position discontinuity between read segments, and microhomology descriptors
608 near candidate junctions. The resulting feature set was restricted to quantities
609 that can be computed from standard BAM/FASTQ files in typical mitochondrial
610 sequencing workflows.

611 The labelled dataset was randomly partitioned into training (80%) and test
612 (20%) subsets using stratified sampling to preserve the 1:1 ratio of clean to
613 chimeric reads. Model development and evaluation were implemented in Python
614 (Version 3.11) using the `scikit-learn`, `xgboost`, `lightgbm`, and `catboost` li-
615 braries. A broad panel of classification algorithms was then benchmarked on the
616 training data to obtain a fair comparison of different model families under identical

617 feature conditions. The panel included: a trivial dummy classifier, L2-regularized
618 logistic regression, a calibrated linear support vector machine (SVM), k -nearest
619 neighbours, Gaussian Naïve Bayes, decision-tree ensembles (Random Forest, Ex-
620 tremely Randomized Trees, and Bagging with decision trees), gradient boosting
621 methods (Gradient Boosting, XGBoost, LightGBM, and CatBoost), and a shallow
622 multilayer perceptron (MLP).

623 For each model, five-fold stratified cross-validation was performed on the train-
624 ing set. In every fold, four-fifths of the data were used for fitting and the remaining
625 one-fifth for validation. Mean cross-validation accuracy, precision, recall, F1-score
626 for the chimeric class, and area under the receiver operating characteristic curve
627 (ROC–AUC) were computed to summarize performance and rank candidate meth-
628 ods. This baseline screen allowed comparison of linear, probabilistic, neural, and
629 ensemble-based approaches and identified tree-based ensemble and boosting mod-
630 els as consistently strong performers relative to simpler baselines.

631 **3.1.4 Model Benchmarking, Hyperparameter Optimiza- 632 tion, and Evaluation**

633 Model selection and refinement proceeded in two stages. First, the cross-validation
634 results from the broad panel were used to identify a subset of competitive mod-
635 els for more detailed optimization. Specifically, ten model families were carried
636 forward: L2-regularized logistic regression, calibrated linear SVM, Random For-
637 est, ExtraTrees, Gradient Boosting, XGBoost, LightGBM, CatBoost, Bagging
638 with decision trees, and a shallow MLP. This subset spans both linear and non-
639 linear decision boundaries, but emphasizes ensemble and boosting methods, which

640 showed superior F1 and ROC–AUC in the initial benchmark.

641 Second, hyperparameter optimization was conducted for each of the ten se-
642 lected models using randomized search with five-fold stratified cross-validation
643 (`RandomizedSearchCV`). For tree-based ensembles, the search space included the
644 number of trees, maximum depth, minimum samples per split and leaf, and the
645 fraction of features considered at each split. For boosting methods, key hyper-
646 parameters such as the number of boosting iterations, learning rate, tree depth,
647 subsampling rate, and column subsampling rate were tuned. For the MLP, the
648 number and size of hidden layers, learning rate, and L_2 regularization strength
649 were varied. In all cases, the primary optimisation criterion was the F1-score of
650 the chimeric class, averaged across folds.

651 For each model family, the hyperparameter configuration with the highest
652 mean cross-validation F1-score was selected as the best-tuned estimator. These
653 tuned models were then refitted on the full training set and evaluated once on the
654 held-out test set to obtain unbiased estimates of performance. Test-set metrics in-
655 cluded accuracy, precision, recall, F1-score for the chimeric class, and ROC–AUC.
656 Confusion matrices and ROC curves were generated for the top-performing mod-
657 els to characterise common error modes, such as false negatives (missed chimeric
658 reads) and false positives (clean reads incorrectly labelled as chimeric). The final
659 model or small set of models for downstream interpretation was chosen based on
660 a combination of test-set F1-score, ROC–AUC, and practical considerations such
661 as model complexity and ease of deployment within a feature extraction pipeline.

662 3.1.5 Feature Importance and Interpretation

663 To relate model decisions to biologically meaningful signals, feature-importance
664 analyses were performed on the best-performing tree-based models. Two comple-
665 mentary approaches were used. First, built-in importance measures from ensemble
666 methods (e.g., split-based importances in Random Forest and Gradient Boosting)
667 were examined to obtain an initial ranking of features based on their contribution
668 to reducing impurity. Second, model-agnostic permutation importance was com-
669 puted on the test set by repeatedly permuting each feature column while keeping
670 all others fixed and measuring the resulting decrease in F1-score. Features whose
671 permutation led to a larger performance drop were interpreted as more influential
672 for chimera detection.

673 For interpretability, individual features were grouped into four conceptual
674 families: (i) supplementary alignment and alignment-structure features (e.g., SA
675 count, spacing between alignment segments, strand consistency), (ii) CIGAR-
676 derived soft-clipping features (e.g., left and right soft-clipped length, total clipped
677 bases), (iii) k-mer composition discontinuity features (e.g., cosine distance and
678 Jensen–Shannon divergence between k-mer profiles of read segments), and (iv) mi-
679 crohomology descriptors (e.g., microhomology length and local GC content around
680 putative breakpoints). Aggregating permutation importance scores within each
681 family allowed assessment of which biological signatures contributed most strongly
682 to the classifier’s performance. This analysis provided a basis for interpreting the
683 trained models in terms of known mechanisms of PCR-induced template switching
684 and for identifying which alignment- and sequence-derived cues are most informa-
685 tive for distinguishing chimeric from clean mitochondrial reads.

686 **3.1.6 Validation and Testing**

687 Validation will involve both internal and external evaluations. Internal valida-
688 tion was achieved through five-fold cross-validation on the training data to verify
689 model generalization and reduce variance due to random sampling. External vali-
690 dation will be achieved through testing on the 20% hold-out dataset derived from
691 the simulated reads, which will be an unbiased benchmark to evaluate how well
692 the trained models generalized to unseen data. All feature extraction and prepro-
693 cessing steps were performed using the same feature extraction pipeline to ensure
694 consistency and comparability across validation stages.

695 Comparative evaluation was performed across all candidate algorithms, in-
696 cluding a trivial dummy classifier, L2-regularized logistic regression, a calibrated
697 linear SVM, k-nearest neighbours, Gaussian Naïve Bayes, decision-tree ensembles,
698 gradient boosting methods, and a shallow MLP. This evaluation determined which
699 models demonstrated the highest predictive performance and computational effi-
700 ciency under identical data conditions. Their metrics were compared to identify
701 which algorithms were most suitable for further refinement.

702 **3.1.7 Documentation**

703 Comprehensive documentation was maintained throughout the study to ensure
704 transparency and reproducibility. All stages of the research, including data gath-
705 ering, preprocessing, feature extraction, model training, and validation, were sys-
706 tematically recorded in a `.README` file in the GitHub repository. For each ana-
707 lytical step, the corresponding parameters, software versions, and command line

708 scripts were documented to enable exact replication of results.

709 The repository structure followed standard research data management practices,
710 with clear directories for datasets and scripts. Computational environments
711 were standardized using Conda, with an environment file (`environment.arm.yml`)
712 specifying dependencies and package versions to maintain consistency across sys-
713 tems.

714 For manuscript preparation and supplementary materials, Overleaf (L^AT_EX)
715 was used to produce publication-quality formatting and consistent referencing. f

716 3.2 Calendar of Activities

717 Table 3.1 presents the project timeline in the form of a Gantt chart, where each
718 bullet point corresponds to approximately one week of planned activity.

Table 3.1: Timetable of Activities

Activities (2025)	Nov	Dec	Jan	Feb	Mar	Apr	May
Data Collection and Simulation	• • •						
Feature Extraction Pipeline			• • •	• • •			
Machine Learning Development			••	• • •	• • •	••	
Testing and Validation						••	• • •
Documentation	• • •	• • •	• • •	• • •	• • •	• • •	• • •

719 Chapter 4

720 Results and Discussion

721 4.1 Descriptive Analysis of Features

722 This chapter presents the performance of the proposed feature set and machine-
723 learning models for detecting PCR-induced chimeric reads in simulated mitochon-
724 drial Illumina data. We first describe the behaviour of the main features, then
725 compare baseline classifiers, assess the effect of hyperparameter tuning, and fi-
726 nally analyse feature importance in terms of individual variables and biologically
727 motivated feature families.

728 The final dataset contained 31 986 reads for training and 7 997 reads for testing,
729 with classes balanced (approximately 4 000 clean and 4 000 chimeric reads in the
730 test split).

731 4.1.1 Univariate Distributions

732 The kernel density plots in Figures 4.1a–4.1f collectively show that alignment-
733 based features provide the strongest separation between clean and chimeric reads.
734 The distribution of `sa_count` (Figure 4.1a) is distinctly bimodal, with clean reads
735 concentrated near zero and chimeric reads peaking around one, reflecting the
736 frequent presence of supplementary alignments in chimeras. A similar pattern of
737 clear separation is observed in `softclip_left` and `softclip_right` (Figures 4.1c
738 and 4.1d), where clean reads cluster tightly at zero while chimeric reads display
739 broad, long-tailed distributions, consistent with extensive soft clipping when
740 a read spans multiple genomic locations. In contrast, `microhomology_length`
741 (Figure 4.1b) shows substantial overlap between classes, with both distribu-
742 tions sharply concentrated near zero and exhibiting smaller secondary peaks
743 at short integer lengths, indicating limited discriminative value under the sim-
744 ulated conditions. Finally, the k-mer-based features `kmer_js_divergence` and
745 `kmer_cosine_diff` (Figures 4.1e and 4.1f) exhibit highly overlapping, multimodal
746 distributions with both classes peaking near 1.0; although chimeric reads appear
747 slightly less concentrated at the highest similarity values, the separation is weak
748 overall.

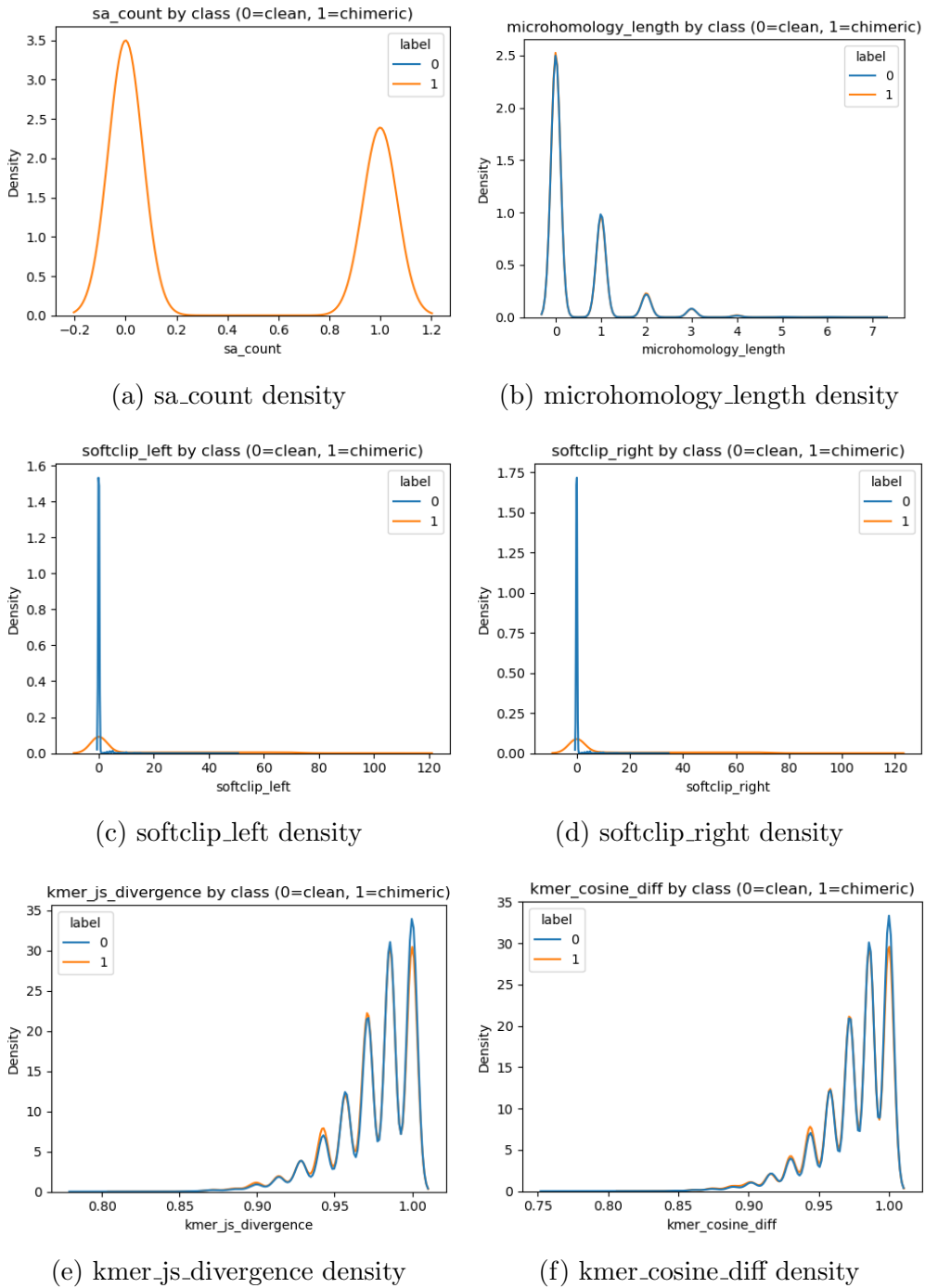


Figure 4.1: Kernel density plots of six key features comparing clean and chimeric reads.

749 4.2 Baseline Classification Performance

750 Table 4.1 summarises the performance of eleven classifiers trained on the engi-
751 neered feature set using five-fold cross-validation and evaluated on the held-out
752 test set. All models were optimised using default hyperparameters, without ded-
753 icated tuning.

754 The dummy baseline, which always predicts the same class regardless of the
755 input features, achieved an accuracy of 0.50 and test F1-score of 0.67. This re-
756 flects the balanced class distribution and provides a lower bound for meaningful
757 performance.

758 Across other models, test F1-scores clustered in a narrow band between ap-
759 proximately 0.74 and 0.77 and ROC–AUC values between 0.82 and 0.84. Gradi-
760 ent boosting, CatBoost, LightGBM, XGBoost, bagging trees, random forest, and
761 multilayer perceptron (MLP) all produced very similar scores, with CatBoost and
762 gradient boosting slightly ahead (test F1 \approx 0.77, ROC–AUC \approx 0.84). Linear
763 models (logistic regression and calibrated linear SVM) performed only marginally
764 worse (test F1 \approx 0.74), while Gaussian Naive Bayes lagged behind with substan-
765 tially lower F1 (\approx 0.65) despite very high precision for the chimeric class.

Table 4.1: Performance of baseline classifiers on the held-out test set.

model	test_accuracy	test_precision	test_recall	test_f1	test_roc_auc
dummy_baseline	0.500000	0.500000	1.000000	0.667000	0.500000
logreg_l2	0.789000	0.945000	0.614000	0.744000	0.821000
linear_svm_calibrated	0.789000	0.945000	0.614000	0.744000	0.820000
random_forest	0.788000	0.894000	0.654000	0.755000	0.834000
extra_trees	0.788000	0.901000	0.647000	0.753000	0.824000
gradient_boosting	0.802000	0.936000	0.648000	0.766000	0.840000
xgboost	0.800000	0.929000	0.650000	0.765000	0.839000
lightgbm	0.799000	0.926000	0.650000	0.764000	0.838000
catboost	0.803000	0.936000	0.650000	0.767000	0.839000
knn	0.782000	0.892000	0.642000	0.747000	0.815000
gaussian_nb	0.741000	0.996000	0.483000	0.651000	0.819000
bagging_trees	0.792000	0.900000	0.657000	0.760000	0.837000
mlp	0.789000	0.931000	0.625000	0.748000	0.819000

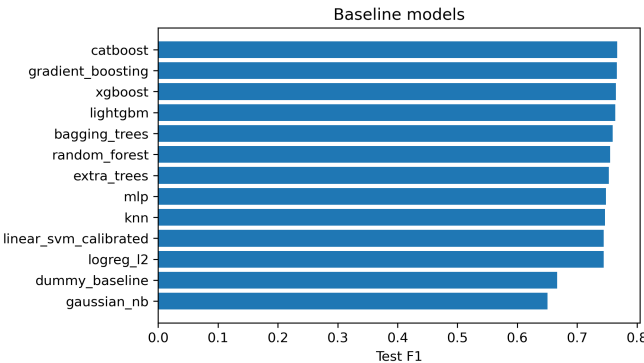


Figure 4.2: Test F1 of all baseline classifiers, showing that no single model clearly dominates and several achieve comparable performance.

766 4.3 Effect of Hyperparameter Tuning

767 To assess whether performance could be improved further, ten model families un-
 768 derwent randomised hyperparameter search (Chapter 3). The tuned metrics are
 769 summarised in Table 4.2. Overall, tuning yielded modest but consistent gains for
 770 tree-based ensembles and boosting methods, while leaving linear models essen-

771 tially unchanged or slightly worse.

772 CatBoost, gradient boosting, LightGBM, XGBoost, random forest, bagging
773 trees, and MLP all experienced small increases in test F1 (typically $\Delta F1 \approx 0.002 -$
774 0.009) and ROC–AUC (up to $\Delta AUC \approx 0.008$). After tuning, CatBoost remained
775 the best performer with test accuracy 0.802, precision 0.924, recall 0.658, F1-score
776 0.769, and ROC–AUC 0.844. Gradient boosting achieved almost identical perfor-
777 mance (F1 0.767, AUC 0.843). Random forest and bagging trees also improved
778 to F1 scores around 0.763 with AUC ≈ 0.842 .

Table 4.2: Performance of tuned classifiers on the held-out test set.

model	test_accuracy	test_precision	test_recall	test_f1	test_roc_auc
logreg_l2_tuned	0.788000	0.946000	0.612000	0.743000	0.818000
linear_svm_calibrated_tuned	0.788000	0.944000	0.612000	0.743000	0.818000
random_forest_tuned	0.797000	0.915000	0.655000	0.763000	0.842000
extra_trees_tuned	0.794000	0.910000	0.652000	0.760000	0.837000
gradient_boosting_tuned	0.802000	0.928000	0.654000	0.767000	0.843000
xgboost_tuned	0.799000	0.922000	0.653000	0.765000	0.839000
lightgbm_tuned	0.801000	0.930000	0.651000	0.766000	0.842000
catboost_tuned	0.802000	0.924000	0.658000	0.769000	0.844000
bagging_trees_tuned	0.798000	0.922000	0.650000	0.763000	0.842000
mlp_tuned	0.790000	0.934000	0.625000	0.749000	0.821000

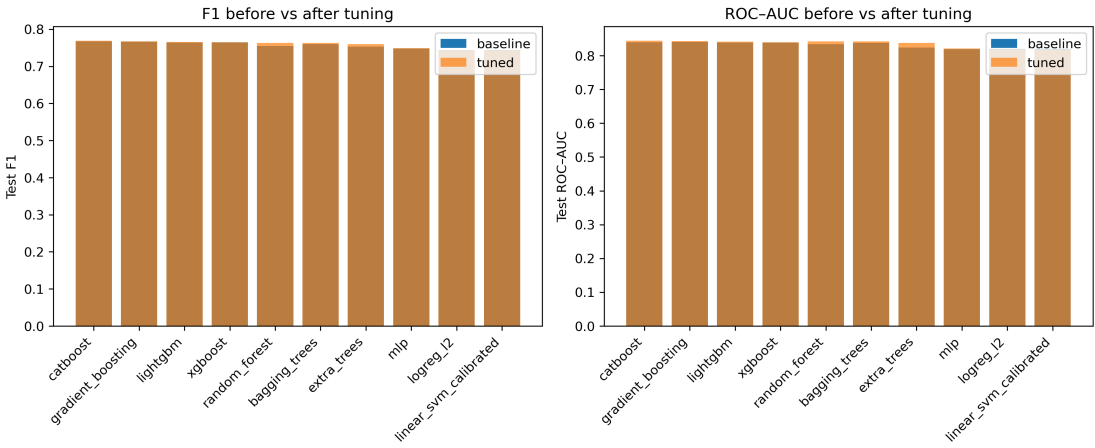


Figure 4.3: Comparison of test F1 (left) and ROC–AUC (right) for baseline and tuned models. Hyperparameter tuning yields small but consistent gains, particularly for tree-based ensembles.

779 Because improvements are small and within cross-validation variability, we
 780 interpret tuning as stabilising and slightly refining the models rather than funda-
 781 mentally altering their behaviour or their relative ranking.

782 4.4 Detailed Evaluation of Representative Mod- 783 els

784 For interpretability and diversity, four tuned models were selected for deeper
 785 analysis: CatBoost (best-performing boosted tree), scikit-learn gradient boost-
 786 ing (canonical gradient-boosting implementation), random forest (non-boosted
 787 ensemble baseline), and L2-regularised logistic regression (linear baseline). All
 788 models were trained on the engineered feature set and evaluated on the same
 789 held-out test data.

790 4.4.1 Confusion Matrices and Error Patterns

791 Classification reports and confusion matrices for the four models reveal consistent
792 patterns. CatBoost and gradient boosting both reached overall accuracy of ap-
793 proximately 0.80 with similar macro-averaged F1 scores (~ 0.80). For CatBoost,
794 precision and recall for clean reads were 0.73 and 0.95, respectively, while for
795 chimeric reads they were 0.92 and 0.66 (F1 = 0.77). Gradient boosting showed
796 nearly identical trade-offs.

797 Random forest attained slightly lower accuracy (0.80) and chimeric F1 (0.76),
798 whereas logistic regression achieved the lowest accuracy among the four (0.79)
799 and chimeric F1 (0.74), although it provided the highest chimeric precision (0.95)
800 at the cost of lower recall (0.61).

801 Across all models, errors were asymmetric. False negatives (chimeric reads
802 predicted as clean) were more frequent than false positives. For example, CatBoost
803 misclassified 1 369 chimeric reads as clean but only 215 clean reads as chimeric.
804 This pattern indicates that the models are conservative: they prioritise avoiding
805 spurious chimera calls at the expense of missing some true chimeras. Depending on
806 downstream application, alternative decision thresholds or cost-sensitive training
807 could be explored to adjust this balance.

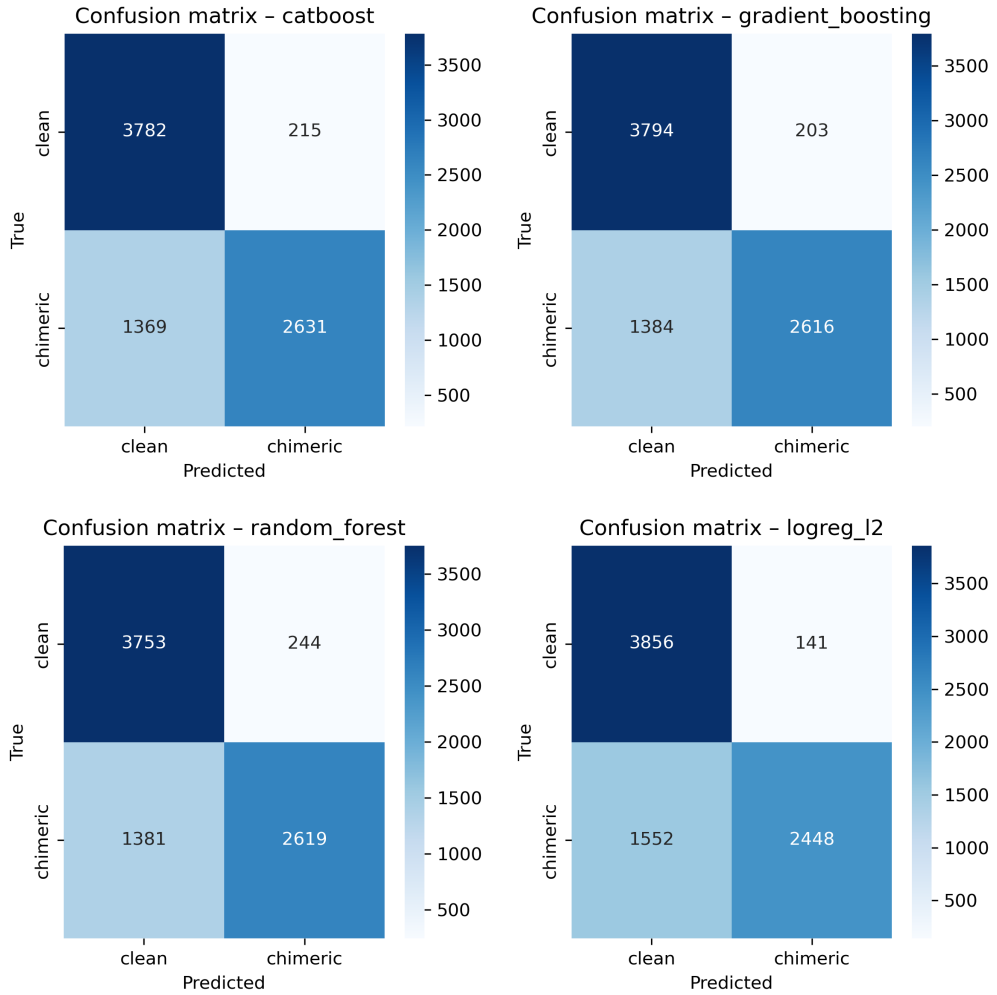


Figure 4.4: Confusion matrices for the four representative models on the held-out test set. All models show more false negatives (chimeric reads called clean) than false positives.

808 4.4.2 ROC and Precision–Recall Curves

809 Receiver operating characteristic (ROC) and precision–recall (PR) curves (Fig-
 810 ure 4.5) further support the similarity among the top models. The three tree-based
 811 ensembles (CatBoost, gradient boosting, random forest) achieved ROC–AUC val-
 812 ues of approximately 0.84 and average precision (AP) around 0.88. Logistic re-

813 gression performed slightly worse ($AUC \approx 0.82$, $AP \approx 0.87$) but still substantially
814 better than random guessing.

815 The PR curves show that precision remains above 0.9 across a broad range
816 of recall values (up to roughly 0.5–0.6), after which precision gradually declines.
817 This behaviour indicates that the models can assign very high confidence to a
818 subset of chimeric reads, while more ambiguous reads can only be recovered by
819 accepting lower precision.

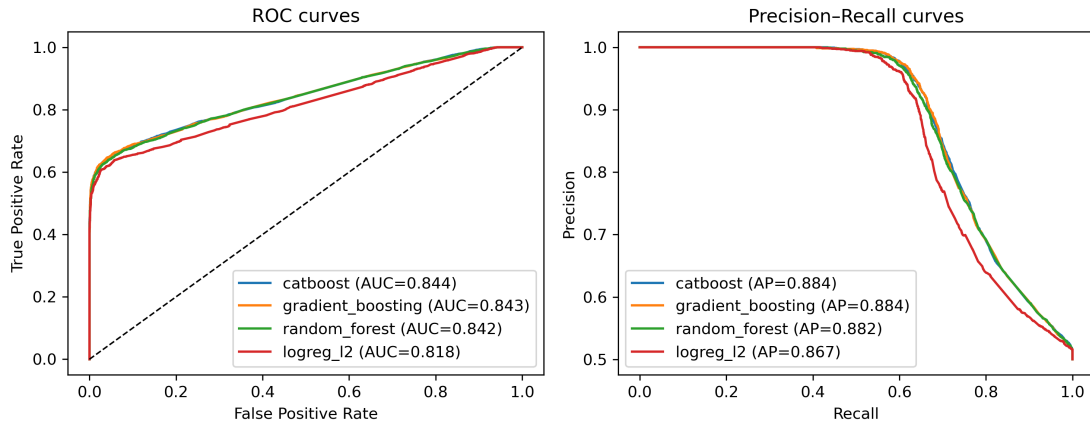


Figure 4.5: ROC (left) and precision–recall (right) curves for the four representative models on the held-out test set. Tree-based ensembles cluster closely, with logistic regression performing slightly but consistently worse.

820 **4.5 Feature Importance and Biological Interpre-**
821 **tation**

822 **4.5.1 Permutation Importance of Individual Features**

823 To understand how each classifier made predictions, feature importance was quan-
824 tified using permutation importance. In this approach, the values of a single fea-
825 ture are randomly shuffled, and the resulting drop in F_1 score (ΔF_1) reflects how
826 strongly the model depends on that feature. Greater decreases in F_1 indicate
827 stronger reliance on that feature. This analysis was applied to four representa-
828 tive models: CatBoost, Gradient Boosting, Random Forest, and L_2 -regularized
829 Logistic Regression.

830 As shown in Figure 4.6, the total number of clipped bases consistently pro-
831 vides a strong predictive signal, particularly in Random Forest, Gradient Boosting,
832 and L_2 -regularized Logistic Regression. CatBoost differs by assigning the highest
833 importance to k-mer divergence metrics such as `kmer_js_divergence`, which cap-
834 ture subtle sequence changes resulting from structural variants or PCR-induced
835 chimeras. Soft-clipping features (`softclip_left` and `softclip_right`) provide
836 additional context around breakpoints, complementing these primary signals in
837 all models except Gradient Boosting. L_2 -regularized Logistic Regression relies
838 more on alignment-based split-read metrics when breakpoints are simple, but it is
839 less effective at detecting complex rearrangements that introduce novel sequences.

840 Overall, these results indicate that accurate detection of chimeric reads relies
841 on both alignment-based signals and k-mer compositional information. Explicit

842 microhomology features contribute minimally in this analysis, and combining both
 843 alignment-based and sequence-level features enhances model sensitivity and speci-
 844 ficity.

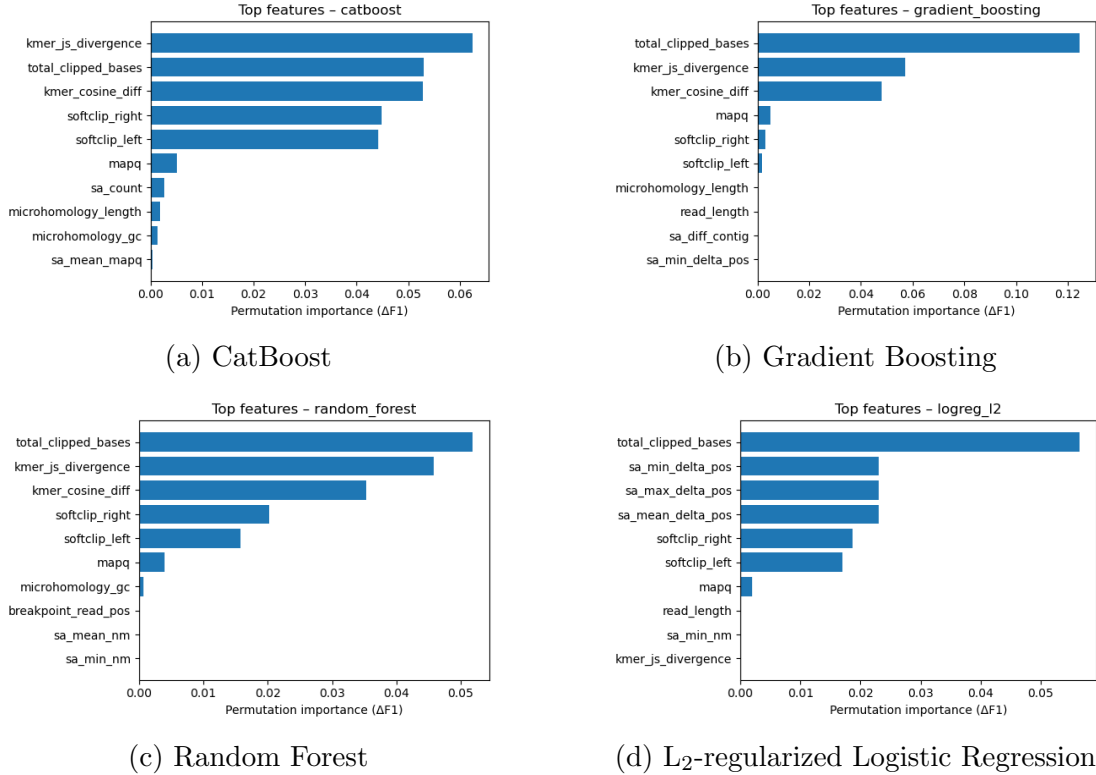


Figure 4.6: Permutation-based feature importance for four representative classifiers. Clipping and k-mer composition features are generally the strongest predictors, whereas microhomology and other alignment metrics contribute minimally.

845 4.5.2 Feature Family Importance

846 To evaluate the contribution of broader biological signals, features were
 847 grouped into five families: SA_structure (supplementary alignment and seg-
 848 ment metrics, e.g., has_sa, sa_count, sa_min_delta_pos, sa_mean_nm), Clipping
 849 (softclip_left, softclip_right, total_clipped_bases, breakpoint_read_pos),

850 Kmer_jump (`kmer_cosine_diff`, `kmer_js_divergence`), Micro_homology, and
851 Other (e.g., `mapq`).

852 Aggregated analyses reveal consistent patterns across models. In CatBoost,
853 the Clipping family has the largest cumulative contribution (0.14), followed
854 by Kmer_jump (0.12), with Other features contributing modestly (0.005) and
855 SA_structure (0.003) and Micro_homology (0.003) providing minimal predictive
856 power. Gradient Boosting shows a similar trend, with Clipping (0.13) domi-
857 nating, Kmer_jump (0.11) secondary, and the remaining families contributing
858 negligibly. Random Forest integrates both Clipping (0.088) and Kmer_jump
859 (0.08) effectively, while SA_structure, Micro_homology, and Other remain minor
860 contributors. L₂-regularized Logistic Regression emphasizes Clipping (0.09)
861 and SA_structure (0.07), with Kmer_jump and Micro_homology having minimal
862 impact.

863 Both feature-level and aggregated analyses indicate that detection of chimeric
864 reads in this dataset relies primarily on alignment disruptions (Clipping) and
865 k-mer compositional shifts (Kmer_jump), which often arise from PCR-induced
866 recombination events, while explicit microhomology features contribute minimally.

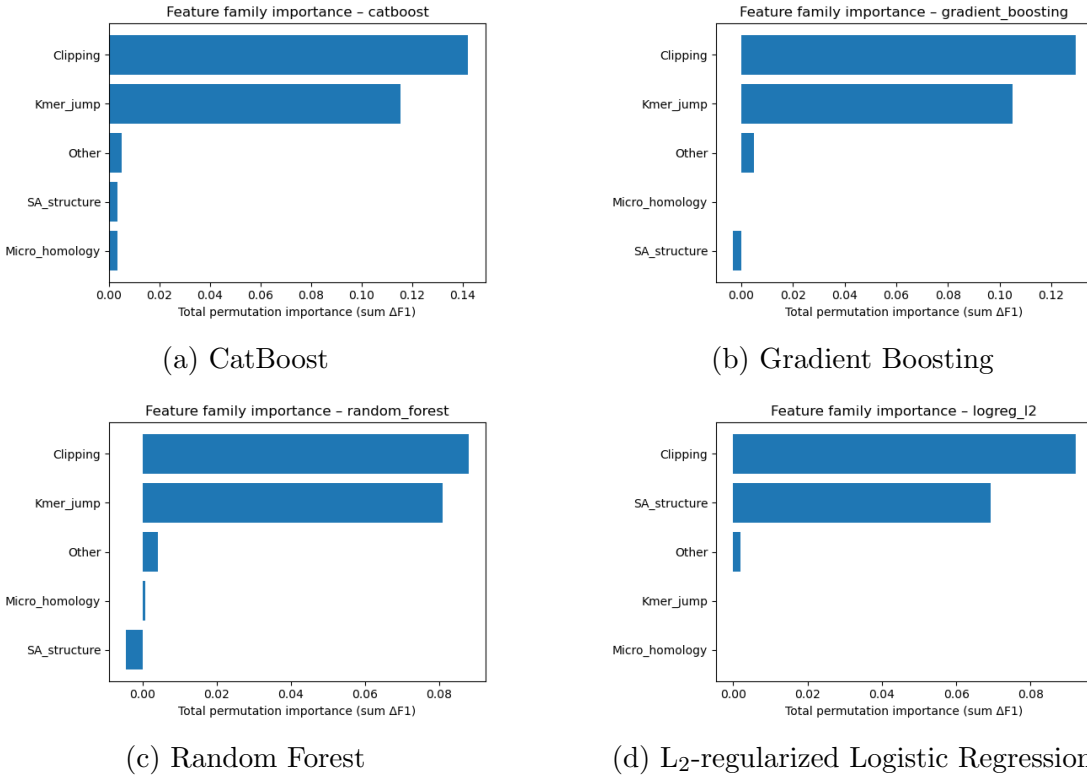


Figure 4.7: Aggregated feature family importance across four models. Clipping and k-mer compositional shifts are consistently the dominant contributors, while SA_structure, Micro_homology, and other features contribute minimally.

867 4.6 Summary of Findings

868 After removing trivially discriminative metadata, all models performed substan-
 869 tially better than the dummy baseline, with test F1-scores around 0.76 and ROC-
 870 AUC values near 0.84. Hyperparameter tuning yielded modest improvements,
 871 with boosting methods, particularly CatBoost and gradient boosting, achieving
 872 the highest performance. Confusion matrices and precision-recall curves indicate
 873 that these models prioritise precision for chimeric reads while accepting lower re-
 874 call, which a conservative strategy appropriate for scenarios where false positives

875 are costly.

876 Feature importance analyses revealed that alignment disruptions, such as clip-
877 ping, and abrupt k-mer composition changes accounted for most predictive power.
878 In contrast, microhomology metrics and supplementary alignment descriptors con-
879 tributed minimally. These results indicate that features based on read alignment
880 and k-mer composition are sufficient to train classifiers for detecting mitochon-
881 drial PCR-induced chimera reads, without needing additional quality-score or
882 positional information in the conditions tested.

⁸⁸³ References

- ⁸⁸⁴ Anderson, S., Bankier, A., Barrell, B., Bruijn, M., Coulson, A., Drouin, J., ...
⁸⁸⁵ Young, I. (1981, 04). Sequence and organization of the human mitochondrial
⁸⁸⁶ genome. *Nature*, *290*, 457-465. doi: 10.1038/290457a0
- ⁸⁸⁷ Arango, G., Garner, E., Pruden, A., Heath, L., Vikesland, P., & Zhang, L. (2018,
⁸⁸⁸ 02). Deeparg: A deep learning approach for predicting antibiotic resistance
⁸⁸⁹ genes from metagenomic data. *Microbiome*, *6*. doi: 10.1186/s40168-018
⁸⁹⁰ -0401-z
- ⁸⁹¹ Bentley, D. R., Balasubramanian, S., Swerdlow, H. P., Smith, G. P., Milton, J.,
⁸⁹² Brown, C. G., ... Smith, A. J. (2008). Accurate whole human genome
⁸⁹³ sequencing using reversible terminator chemistry. *Nature*, *456*(7218), 53–
⁸⁹⁴ 59. doi: 10.1038/nature07517
- ⁸⁹⁵ Boore, J. L. (1999). Animal mitochondrial genomes. *Nucleic Acids Research*,
⁸⁹⁶ *27*(8), 1767–1780. doi: 10.1093/nar/27.8.1767
- ⁸⁹⁷ Cameron, S. L. (2014). Insect mitochondrial genomics: Implications for evolution
⁸⁹⁸ and phylogeny. *Annual Review of Entomology*, *59*, 95–117. doi: 10.1146/
⁸⁹⁹ annurev-ento-011613-162007
- ⁹⁰⁰ Dierckxsens, N., Mardulyn, P., & Smits, G. (2017). Novoplasty: de novo assembly
⁹⁰¹ of organelle genomes from whole genome data. *Nucleic Acids Research*,

- 902 45(4), e18. doi: 10.1093/nar/gkw955
- 903 Edgar, R. C. (2016). Uchime2: improved chimera prediction for amplicon se-
904 quencing. *bioRxiv*. Retrieved from <https://api.semanticscholar.org/>
905 CorpusID:88955007
- 906 Edgar, R. C. (n.d.). *Uchime in practice*. Retrieved from https://www.drive5.com/usearch/manual7/uchime_practical.html
- 907 Edgar, R. C., Haas, B. J., Clemente, J. C., Quince, C., & Knight, R. (2011).
908 Uchime improves sensitivity and speed of chimera detection. *Bioinformatics*,
909 27(16), 2194–2200. doi: 10.1093/bioinformatics/btr381
- 910 Glenn, T. C. (2011). Field guide to next-generation dna sequencers. *Molecular
911 Ecology Resources*, 11(5), 759–769. doi: 10.1111/j.1755-0998.2011.03024.x
- 912 Gonzalez, J. M., Zimmermann, J., & Saiz-Jimenez, C. (2004, 09). Evalu-
913 ating putative chimeric sequences from pcr-amplified products. *Bioin-
914 formatics*, 21(3), 333-337. Retrieved from <https://doi.org/10.1093/bioinformatics/bti008>
915 doi: 10.1093/bioinformatics/bti008
- 916 Gray, M. W. (2012). Mitochondrial evolution. *Cold Spring Harbor perspectives
917 in biology*, 4. Retrieved from <https://doi.org/10.1101/cshperspect.a011403>
918 doi: 10.1101/cshperspect.a011403
- 919 Hahn, C., Bachmann, L., & Chevreux, B. (2013). Reconstructing mitochondrial
920 genomes directly from genomic next-generation sequencing reads—a baiting
921 and iterative mapping approach. *Nucleic Acids Research*, 41(13), e129. doi:
922 10.1093/nar/gkt371
- 923 Jin, J.-J., Yu, W.-B., Yang, J., Song, Y., dePamphilis, C. W., Yi, T.-S., & Li,
924 D.-Z. (2020). Getorganelle: a fast and versatile toolkit for accurate de
925 novo assembly of organelle genomes. *Genome Biology*, 21(1), 241. doi:
926 10.1186/s13059-020-02154-5
927

- 928 Judo, M. S. B., Wedel, W. R., & Wilson, B. H. (1998). Stimulation and sup-
929 pression of pcr-mediated recombination. *Nucleic Acids Research*, *26*(7),
930 1819–1825. doi: 10.1093/nar/26.7.1819
- 931 Labrador, K., Agmata, A., Palermo, J. D., Ravago-Gotanco, R., & Pante, M. J.
932 (2021). Mitochondrial dna reveals genetically structured haplogroups of
933 bali sardinella (sardinella lemuru) in philippine waters. *Regional Studies in*
934 *Marine Science*, *41*, 101588. doi: 10.1016/j.rsma.2020.101588
- 935 Layer, R., Hall, I., & Quinlan, A. (2014, 10). Lumpy: A probabilistic framework
936 for structural variant discovery. *Genome Biology*, *15*. doi: 10.1186/gb-2014
937 -15-6-r84
- 938 Li, H. (2018, 05). Minimap2: pairwise alignment for nucleotide sequences. *Bioin-*
939 *formatics*, *34*(18), 3094-3100. Retrieved from <https://doi.org/10.1093/bioinformatics/bty191>
940 doi: 10.1093/bioinformatics/bty191
- 941 Liang, Q., Bible, P. W., Liu, Y., Zou, B., & Wei, L. (2020, 02). Deepmi-
942 crobes: taxonomic classification for metagenomics with deep learning. *NAR*
943 *Genomics and Bioinformatics*, *2*(1), lqaa009. Retrieved from <https://doi.org/10.1093/nargab/lqaa009>
944 doi: 10.1093/nargab/lqaa009
- 945 Metzker, M. L. (2010). Sequencing technologies — the next generation. *Nature*
946 *Reviews Genetics*, *11*(1), 31–46. doi: 10.1038/nrg2626
- 947 Mysara, M., Saeys, Y., Leys, N., Raes, J., & Monsieurs, P. (2015). Catch,
948 an ensemble classifier for chimera detection in 16s rrna sequencing stud-
949 ies. *Applied and Environmental Microbiology*, *81*(5), 1573-1584. Retrieved
950 from <https://journals.asm.org/doi/abs/10.1128/aem.02896-14> doi:
951 10.1128/AEM.02896-14
- 952 Peccoud, J., Lequime, S., Moltini-Conclois, I., Giraud, I., Lambrechts, L., &
953 Gilbert, C. (2018, 04). A survey of virus recombination uncovers canon-

- 954 ical features of artificial chimeras generated during deep sequencing li-
955 brary preparation. *G3 Genes—Genomes—Genetics*, 8(4), 1129-1138. Re-
956 trieval from <https://doi.org/10.1534/g3.117.300468> doi: 10.1534/
957 g3.117.300468
- 958 Qin, Y., Wu, L., Zhang, Q., Wen, C., Nostrand, J. D. V., Ning, D., ... Zhou, J.
959 (2023). Effects of error, chimera, bias, and gc content on the accuracy of
960 amplicon sequencing. *mSystems*, 8(6), e01025-23. Retrieved from <https://journals.asm.org/doi/abs/10.1128/msystems.01025-23> doi: 10.1128/
961 msystems.01025-23
- 962 Qiu, X., Wu, L., Huang, H., McDonel, P. E., Palumbo, A. V., Tiedje, J. M., &
963 Zhou, J. (2001). Evaluation of pcr-generated chimeras, mutations, and het-
964 eroduplexes with 16s rrna gene-based cloning. *Applied and Environmental
965 Microbiology*, 67(2), 880–887. doi: 10.1128/AEM.67.2.880-887.2001
- 966 Ren, J., Song, K., Deng, C., Ahlgren, N., Fuhrman, J., Li, Y., ... Sun, F. (2020,
967 01). Identifying viruses from metagenomic data using deep learning. *Quan-
968 titative Biology*, 8. doi: 10.1007/s40484-019-0187-4
- 969 Rodriguez-Martin, B., Palumbo, E., Marco-Sola, S., Griebel, T., Ribeca, P.,
970 Alonso, G., ... Djebali, S. (2017, 01). Chimpipe: Accurate detection of
971 fusion genes and transcription-induced chimeras from rna-seq data. *BMC
972 Genomics*, 18. doi: 10.1186/s12864-016-3404-9
- 973 Rognes, T., Flouri, T., Nichols, B., Quince, C., & Mahé, F. (2016). Vsearch: a
974 versatile open source tool for metagenomics. *PeerJ*, 4, e2584. doi: 10.7717/
975 peerj.2584
- 976 Sedlazeck, F., Rescheneder, P., Smolka, M., Fang, H., Nattestad, M., von Haeseler,
977 A., & Schatz, M. (2018, 06). Accurate detection of complex structural
978 variations using single-molecule sequencing. *Nature Methods*, 15. doi: 10

- 980 .1038/s41592-018-0001-7
- 981 982 983 984 985 Sfeir, A., & Symington, L. S. (2015). Microhomology-mediated end joining: A back-up survival mechanism or dedicated pathway? *Trends in Biochemical Sciences*, 40(11), 701-714. Retrieved from <https://www.sciencedirect.com/science/article/pii/S0968000415001589> doi: <https://doi.org/10.1016/j.tibs.2015.08.006>
- 986 987 988 989 Vervier, K., Mahé, P., Tournoud, M., Veyrieras, J.-B., & Vert, J.-P. (2015, 11). Large-scale machine learning for metagenomics sequence classification. *Bioinformatics*, 32(7), 1023-1032. Retrieved from <https://doi.org/10.1093/bioinformatics/btv683> doi: 10.1093/bioinformatics/btv683
- 990 991 992 993 Willette, D., Bognot, E., Mutia, M. T., & Santos, M. (2011). *Biology and ecology of sardines in the philippines: A review* (Vol. 13; Tech. Rep. No. 1). NFRDI Technical Paper Series. Retrieved from <https://nfrdi.da.gov.ph/tpjf/etc/Willette%20et%20al.%20Sardines%20Review.pdf>